Motion and Muscle Artifact Removal Validation Using an Electrical Head Phantom, Robotic Motion Platform, and Dual Layer Mobile EEG

Natalie Richer, Ryan J. Downey, W. David Hairston, *Member, IEEE*, Daniel P. Ferris, *Senior Member, IEEE*, and Andrew D. Nordin, *Member, IEEE*

***Abstract*— Motion and muscle artifacts can undermine signal quality in electroencephalography (EEG) recordings during locomotion. We evaluated approaches for recovering ground-truth artificial brain signals from noisy EEG recordings. We built an electrical head phantom that broadcast four brain and four muscle sources. Head movements were generated by a robotic motion platform. We recorded 128-channel dual layer EEG and 8-channel neck electromyography (EMG) from the head phantom during motion. We evaluated ground-truth electrocortical source signal recovery from artifact contaminated data using Independent Component Analysis (ICA) to determine: (1) the number of isolated noise sensor recordings needed to capture and remove motion artifacts, (2) the ability of Artifact Subspace Reconstruction to remove motion and muscle artifacts at contrasting artifact detection thresholds, (3) the number of neck EMG sensor recordings needed to capture and remove muscle artifacts, and (4) the ability of Canonical Correlation Analysis to remove muscle artifacts. We also evaluated source signal recovery by combining the best practices identified in aims 1-4. By including isolated noise and EMG recordings in the ICA decomposition, we more effectively recovered ground-truth artificial brain signals. A reduced subset of 32-noise and 6-EMG channels showed equivalent performance compared to including the complete arrays. Artifact Subspace Reconstruction improved source separation, but this was contingent on muscle activity amplitude. Canonical Correlation Analysis also improved source separation. Merging noise and EMG recordings into the ICA decomposition, with Artifact Subspace Reconstruction and Canonical Correlation Analysis preprocessing, improved source signal recovery. This study expands on previous head phantom experiments by including neck muscle source activity and evaluating artificial electrocortical spectral power fluctuations synchronized with gait events.**

Manuscript received November 2, 2019; revised May 27, 2020; accepted June 5, 2020. Date of publication June 9, 2020; date of current version August 7, 2020. This work was supported by the Cognition and Neuroergonomics Collaborative Technology Alliance under Grant ARL W911NF-10-2-0022. *(Corresponding author: Natalie Richer.)*

Natalie Richer, Ryan J. Downey, Daniel P. Ferris, and Andrew D. Nordin are with the J. Crayton Pruitt Family Department of Biomedical Engineering, University of Florida, Gainesville, FL 32611 USA (e-mail: nricher@ufl.edu; rdowney@bme.ufl.edu; dferris@bme.ufl.edu; andrew.nordin@bme.ufl.edu).

W. David Hairston is with the Human Research and Engineering Directorate, United States Army Research Laboratory, Aberdeen Proving Ground, MD 21005 USA (e-mail: william.d.hairston4.civ@mail.mil).

This article has supplementary downloadable material available at http://ieeexplore.ieee.org, provided by the authors.

Digital Object Identifier 10.1109/TNSRE.2020.3000971

***Index Terms*— Electroencephalography, head phantom, motion artifacts, muscle artifacts, signal processing.**

I. Introduction

ELECTROENCEPHALOGRAPHY (EEG) is increasingly recognized as an effective tool for mobile brain imaging because it is portable, lightweight and offers a high temporal resolution [1]. A main limitation, however, is its sensitivity to artifacts caused by motion and muscle activity. Motion of the EEG electrodes during movement can cause voltage fluctuations unrelated to brain activity [2], [3]. Electrodes can also capture physiological signals such as eye blinks and muscle activity of the head and neck. To improve the use of EEG for mobile brain imaging, data collection and processing techniques should carefully isolate electrocortical activity from artifact sources.

Mobile EEG studies reveal electrocortical spectral power fluctuations across the gait cycle [4]–[12]. There are repeated observations of increased alpha (8-12 Hz) and beta (12-30 Hz) spectral power in sensorimotor [8], [9], [12] and motor [10], [11] areas during double support prior to contralateral limb push off, followed by a decrease during swing of the contralateral leg. These observations have been possible thanks to advanced processing methods that help isolate and remove artifacts. Blind source separation, such as adaptive mixture independent component analysis (AMICA), can separate brain activity from motion and confounding physiological artifacts [13]. This approach has been used in many mobile brain imaging experiments to successfully extract electrocortical activity from noisy EEG data [3], [4], [14]–[19]. Other preprocessing methods can help eliminate motion and muscle artifacts, such as Artifact Subspace Reconstruction and Canonical Correlation Analysis. Artifact Subspace Reconstruction uses a Principal Component Analysis based approach and calibration statistics acquired from clean EEG data. It interpolates high variance components that exceed a predetermined threshold relative to clean data and reconstructs the channel data [20], [21]. It has been widely used to successfully remove EEG artifacts [11], [12], [16], [20]–[23]. However, care must be taken when selecting the artifact detection threshold as an aggressive cutoff can remove brain activity as well as artifacts [11]. Canonical Correlation Analysis has

subsequently been used to decompose EEG channel data based on autocorrelation. Components with unusually low autocorrelation that capture high frequency electrical and muscle artifacts can therefore be extracted to reconstruct clean scalp EEG recordings [12], [16], [24]–[27].

Because the underlying electrocortical source activity is largely unknown in human mobile EEG recordings, it is useful to evaluate the performance of blind source separation and other preprocessing methods in comparison to ground-truth signals. By using an electrical head phantom device with embedded antennae for broadcasting simulated brain activity, it is possible to evaluate data collection and signal processing approaches. Head phantom experiments have been used to validate the ability of independent component analysis (ICA) to isolate simple sinusoidal bursts [19] and more complex neural signals [15] from motion-contaminated data. Recent head phantom experiments have also evaluated the influence of mobile EEG hardware configurations and processing techniques for reducing motion artifacts. Symeonidou and colleagues [28] demonstrated the detrimental effect of cable sway on signal-to-noise ratio, underscoring the need to minimize cable movements in a wired EEG setup. Nordin and colleagues [29] subsequently developed dual layer EEG hardware for isolating and removing motion artifacts from mobile EEG recordings. This approach relies on conventional scalp interfacing EEG electrodes along with mechanically coupled and inverted noise-only electrodes that are electrically isolated from the primary sensors [29]. Dual layer EEG hardware and signal processing has been evaluated during motion using electrical head phantom devices [17], [29] and has been used to uncover human brain dynamics during obstacle navigation and at different gait speeds [12], [17]. Ground-truth signal cleaning comparisons can help establish best practices for mobile EEG artifact removal.

Previous benchmark testing with the head phantom evaluated methods to reduce motion artifacts. During human locomotion, motion and muscle artifacts can each undermine EEG signal quality due to overlapping timing and spectral content with electrocortical activity. Neck muscles are important for stabilization of the head during locomotion [30]. Adding neck muscle sources to our electrical head phantom allows us to objectively assess both motion and muscle artifact-cleaning methods using rigorous benchmark tests [31]. Realistic brain signals that contain gait-related spectral power fluctuations will also allow us to evaluate the influence of our signal cleaning methods on event-related spectral perturbations across the step cycle; a common measure used to evaluate electrocortical dynamics during locomotion.

Our objective was to determine best practices for dual layer mobile EEG hardware configurations and signal processing schemes. We extracted artificial brain signals from mobile EEG recordings contaminated by simulated motion and muscle artifacts using an electrical head phantom and robotic motion platform. From these mobile EEG data, we evaluated ground-truth electrocortical source recovery using ICA to determine: (1) the number of isolated noise sensor recordings needed to capture and remove motion artifacts, (2) the ability of Artifact Subspace Reconstruction to remove motion artifacts at contrasting artifact detection thresholds, (3) the number of neck EMG sensor recordings needed to capture and remove muscle artifacts, and (4) the ability of Canonical Correlation Analysis to remove muscle artifacts. In motion-contaminated data, we hypothesized that including isolated noise recordings from dual layer EEG sensors would help separate motion artifacts from scalp EEG recordings. However, we anticipated that a reduced subset of matched noise pairs could be used to effectively capture and remove the predominant motion-induced noise sources [12], [17]. We also hypothesized that Artifact Subspace Reconstruction preprocessing would remove motion and possibly muscle artifacts [11], [12], [16], [20], but that aggressive artifact identification thresholds could eliminate components of the artificial electrocortical signals. In muscle-contaminated EEG data, we hypothesized that including additional EMG recordings in the ICA decomposition would help to isolate and remove muscle artifacts [8], [12], [17]. Finally, we anticipated that Canonical Correlation Analysis would help capture and remove high-frequency, muscle-induced artifacts [12], [16], [27], [32], [33]. By combining these methods, we predicted that we could cleanly isolate the ground-truth artificial electrocortical sources to assess spectral power fluctuations across the gait cycle.

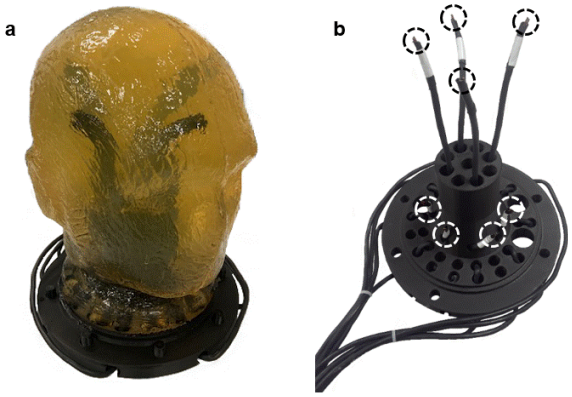

Fig. 1. We built a head phantom from ballistic gelatin (a), surrounding a base with embedded sources (b). Four sources were located at the posterior base of the head to generate muscle activity (b; white circles). Another four were placed in the approximate locations of the frontal, occipital and bilateral sensorimotor cortices (b; black circles).

II. Methods

A. Experimental Setup

We constructed an electrical head phantom device (Fig. 1a) using ballistics gelatin as described in [28] based on a derivative of the model provided under the Open Phantom Project hosted by the Army Research Laboratory (see https://osf.io/qrka2/ [34], [35] for more details). Sodium chloride was added to the gelatin mixture at a concentration of 1% to approximate the ionic conductance of human skin tissue [36]. Ballistics gelatin also resembles the mechanical properties of living tissue [36]–[38]. The head contained an embedded base with eight dipolar sources, each consisting of exposed pairs of wire tips with approximately 2 mm separation (Fig. 1b). Four of these sources were used to generate muscle

activity and were located in the base of the head, in the approximate locations of the left and right sternocleidomastoid and trapezius muscles (Fig. 1b, white circles). The other four sources were used to generate artificial electrocortical source activity (Fig. 1b, black circles). We placed the sources in the approximate location of the left and right sensorimotor cortices, frontal cortex, and occipital cortex. We secured the head to a six-degree of freedom robotic motion platform (Symétrie, Nimes, France) that was used to reproduce human head trajectories recorded during walking.

To generate realistic head motions and electrical neck muscle activity during walking, we collected data from a human subject. A healthy, young male subject (26 years, 170 cm, 62.6 kg) walked at four speeds (0.5, 1.0, 1.5, and 2.0 m/s) on a force-instrumented treadmill (Bertec FIT, Columbus, OH, USA). We recorded data from an inertial measurement unit placed on the subject's forehead (APDM, Portland, OR, USA), band pass filtered (0.5 Hz high-pass, 4 Hz low-pass), and calculated head trajectories that were reproduced by the robotic motion platform. We placed four bipolar surface EMG electrodes (Biometrics Ltd, Ladysmith, VA, USA) on the left and right sternocleidomastoid and trapezius muscles to record neck muscle activity during walking. Muscle activity data were band pass filtered (20 Hz high pass, 300 Hz low pass) and normalized (± 1) to the fastest walking speed (2.0m/s). We used these signals as inputs for the corresponding neck muscle sources in the head phantom. Supplementary Fig. 1 illustrates the spectral power of the muscle inputs as a function of frequency (a) and as a function of the left and right limb heel strike and toe off gait events (c) for the 1.5 m/s walking speed. The event-related spectral perturbation plots demonstrate lateralized high frequency oscillations in spectral power throughout the gait cycle.

To generate complex neuronal activity at a range of physiological frequencies, we used an established neural mass model to simulate human EEG recordings [15], [39], [40]. By combining neural mass models [15], [40], we created four separate complex waveforms with different spectral profiles (Supplementary Fig. 1b). The frontal and occipital artificial electrocortical signals had power spectral density peaks at approximately 7 and 9 Hz, respectively. To add further complexity, the occipital signal also included filtered white noise to create a delta peak at approximately 2.5 Hz. For the sensorimotor signals, we aimed to reproduce spectral power fluctuations synchronized to gait events in alpha (8-12 Hz) and beta (12-30 Hz) bands [4], [12]. For this reason, we combined two signals generated from the neural mass models to create two frequency peaks in each sensorimotor signal. The left sensorimotor cortex signal contained a prominent peak at approximately 12 Hz and a second broader increase in the 20 to 30 Hz range. The right sensorimotor cortex signal contained one prominent peak at approximately 11 Hz and a second moderate increase in the 14 to 16 Hz range. We then produced fluctuations in these sensorimotor signals (Supplementary Fig. 1d) that matched previous human studies showing increased alpha and beta spectral power in sensorimotor cortex during double support prior to push off of the contralateral limb, which decreased during contralateral limb swing [4], [12]. Between left heel strike and right toe off, we increased the alpha and beta activity of the left sensorimotor signal. During the right limb swing, we decreased the alpha and beta activity of the left sensorimotor signal. We performed the same modifications in the right sensorimotor cortex signal in relation to the left limb gait cycle. Artificial brain signal fluctuation amplitudes were normalized (± 1) to allow straightforward scaling when broadcasting the signals through the electrical head phantom. Supplementary Fig. 1 illustrates the spectral power of the artificial electrocortical signals as a function of frequency (b) and as a function of the gait events (d) for the 1.5 m/s walking speed. Importantly, the event-related spectral perturbation plots demonstrate the increases and decreases in spectral power tied to the gait events for the sensorimotor sources, while no gait-related events occur in the frontal and occipital sources, providing positive- and negative-ground truth signals for later evaluation.

Input muscle and brain signals were broadcast through the head phantom using LabVIEW 2018 (National Instruments, Austin, TX, USA) and a National Instruments compact DAQ and output modules (NI cDAQ-9178 and NI-9269, respectively, National Instruments, Austin, TX, USA). Symétrie Motion software (Symétrie, Nimes, France) produced the head motion trajectories that we extracted from human data. We configured a trigger to initiate all input signals simultaneously and indicate the start of the trial in the EEG recording software to ensure all signals were synced and tied to the gait events.

B. Protocol

In a single testing session, we collected 32 experimental trials of 5 minutes each: four muscle amplitude conditions performed with and without motion of the motion platform at each gait speed (0.5, 1.0, 1.5, and 2.0 m/s). Brain signal amplitudes were independently set to yield approximately ± 20 μV at the scalp by measuring the amplitude at the electrode location closest to the source. Muscle amplitudes were similarly set based on measurements at the neck electrodes. We selected four muscle amplitudes: ± 0, 100, 300, and 500 μV based on neck EMG recordings during human walking and running [17]. The ± 0 μV amplitude provided a baseline. The ± 500 μV amplitude was included to provide exaggerated muscle contamination.

C. Electroencephalography Processing

We collected EEG data using a BioSemi Active Two recording system (BSM, BioSemi, Amsterdam, The Netherlands) and a standard 128-channel cap (Electro-Cap International, Inc., Eaton, OH, USA). We inserted conductive gel into each well followed by pin-type Ag/AgCl electrodes. We used an adapted dual layer electrode array [17], [29] with matched noise electrode pairs for all 128 scalp EEG electrodes. The noise electrodes consisted of flat type electrodes mechanically coupled but electrically isolated from the scalp electrodes. We stretched a custom conductive fabric cap (Eeonyx, Pinole, CA) over these electrodes and inserted conductive gel between the electrodes and fabric to form an external artificial

"skin" circuit. Similarly to human experiments, we also placed an additional eight flat-type electrodes over the neck area of the phantom to capture EMG sources separately from EEG. The EMG electrodes used the same reference, ground, and collection box as the primary EEG sensors, while the noise sensors were separately referenced, but synchronously recorded [12], [17]. We arranged the wires to form a single bundle at the back of the head and used hook and loop straps to bundle the ribbon cables leading to the recording systems. Scalp and noise electrode offsets were independently visually inspected to be approximately ±20 mV or below. All signals were recorded at 512 Hz.

Data processing was performed using custom MATLAB 2016b (MathWorks, Inc., Natick, MA, USA) scripts and the EEGLAB toolbox [41]. All data were initially high pass filtered at 1 Hz. Prior to subsequent analyses, we concatenated walking speed condition data separately for each muscle amplitude condition and applied a robust average reference. Unusually noisy channels that remained were then removed using statistical channel rejection criteria (>5 standard deviations from the mean probability distribution and >5 standard deviations from the mean kurtosis). We applied the same procedures separately to neck EMG and isolated noise channel data.

In order to meet the following primary 4 aims, we applied contrasting data preprocessing approaches before performing an AMICA [42]:

(1) Dual layer EEG noise sensor recordings for motion artifact removal: To determine the number of isolated noise sensor recordings needed to capture and remove motion artifacts, we selected different subsets of the isolated noise sensors that were evenly distributed across the scalp. Only contrasting walking speed conditions were considered in this analysis, without neck muscle activity. After preprocessing, we selected isolated noise electrode subsets, including: 0, 32, 64, 96, and 122 noise sensors (the 122 channels that were left after channel rejection). To evaluate the influence of the additional sensor data on the ICA decomposition, we performed AMICA on the complete scalp EEG dataset (after channel rejection), and the subset of isolated noise recordings, by stacking scalp EEG and isolated noise channel data in separate rows of the data matrix [12], [17].

(2) Artifact Subspace Reconstruction for motion and muscle artifact removal: To assess the ability of Artifact Subspace Reconstruction to remove motion and muscle artifacts at contrasting artifact detection thresholds, we ran the preprocessed EEG channel data using Artifact Subspace Reconstruction at four contrasting standard deviation cutoffs from the baseline data, ranging from strict to lenient: 3 standard deviations [10], [22], [23], 10 standard deviations [21], 20 standard deviations [11], [16], and 50 standard deviations [21]. We used a baseline trial that consisted of our cleanest condition (no motion, ±0 μV muscle amplitude, brain signals from the 0.5 m/s walking). When necessary, we excluded channels to ensure similarity between the trial and baseline data. Artifact Subspace Reconstruction preprocessing was completed for each gait speed and muscle amplitude condition individually (±0, 100, 300, and 500 μV), but AMICA was performed on the concatenated gait speed conditions for each muscle amplitude condition separately. For comparison, we also performed AMICA on EEG channel data without Artifact Subspace Reconstruction preprocessing. Only scalp EEG channel data were included in the ICA decomposition for this aim.

(3) Neck EMG sensor recordings for muscle artifact removal: To determine the number of neck EMG recording sensors needed to capture and remove muscle artifacts alone, we selected different subsets of the EMG sensors from the left and right side of the neck. To exclude the influence of motion artifacts, which normally cannot be accomplished during human mobile EEG recordings, our analysis focused on data from conditions where the motion platform remained stationary and muscle input amplitudes were set to ±100 μV. Although the head phantom remained motionless, artificial brain signals from each gait speed condition were broadcast through the head. Subsets of 0, 2, 4, 6, and 8 EMG electrodes were included in the ICA decomposition after preprocessing. We then performed AMICA on the complete scalp EEG dataset (after channel rejection), along with the subset of neck EMG recordings, stacked in separate rows of the data matrix.

(4) Canonical Correlation Analysis for muscle artifact removal: We preprocessed EEG channel data using a Canonical Correlation Analysis based approach to assess its ability to remove contrasting levels of muscle artifacts. Again, the motion platform remained stationary to allow independent assessment of muscle artifact contamination without motion. In each case, data from each gait speed condition were broadcast through the head phantom. We evaluated three separate muscle amplitude conditions: ±100, 300 and 500 μV. Following methods adapted from Nordin *et al*. [12], we used Canonical Correlation Analysis on channel data with a 1-frame lag autocorrelation. Canonical components were separated into low and high frequency content based on autocorrelation, and components with unusually low autocorrelation (high frequency electrical and muscle artifacts) were removed prior to reconstructing the channel data. For comparison, we also performed AMICA on EEG channel data without muscle contamination or Canonical Correlation Analysis processing. Only scalp EEG channel data were included in the ICA decomposition for this aim.

D. Source Signal Recovery Evaluation

By comparing the recovered independent components to our ground-truth input signals, we were able to select the component that best matched the artificial electrocortical source. Specifically, we examined the similarities between the time-frequency features of the input signals and the independent components. To find the best-fit component for each condition, we calculated the root mean square of the difference between the temporally aligned time frequency data for each independent component and the ground-truth artificial brain signal in every gait cycle. We define this as root mean square error. Lower values represent greater similarity to the ground-truth input signal, which suggests better artifact and electrocortical source separation. We specifically evaluated root mean square error in the 8 to 30 Hz frequency range

because our artificial sensorimotor source signals fluctuated in this frequency band.

To provide an unbiased comparison among sources and conditions, we normalized root mean square error to the root mean square of its respective ground-truth spectral power fluctuation pattern for each gait cycle within a condition. We then averaged the normalized root mean square error across gait speeds to identify the best-fit component with the lowest root mean square error compared to the ground-truth signal. We refer to this measure as relative error because it represents the difference between our recovered best-fit component signal and the ground-truth spectral power fluctuations, scaled to the amplitude of the ground-truth spectral power fluctuations. This can be interpreted akin to a noise-to-signal ratio. Relative error values greater than 1 indicate that the error exceeds the spectral power fluctuations of the ground-truth signal. Relative error values equal to 1 indicate the spectral power fluctuations of the error and ground-truth signal are equivalent. Relative error values less than 1 indicate the error is less than the spectral power fluctuations of the ground-truth signal. Zero relative error indicates a perfect match between the best-fit component and the ground-truth spectral power fluctuations.

We evaluated differences among conditions in aims 1-4 using the normalized root mean square error values of the best-fit components. We used the relative error values to calculate 99% confidence intervals from the standard deviation among trials in each condition. Relative error condition comparisons were completed using the aggregated values from the four electrocortical sources.

Although we recorded high density mobile EEG from an expanded dual layer EEG electrode array that was comprised of 128-scalp EEG channels, 128-isolated noise channels, and 8-neck EMG channels (264-total channels), our head phantom contained eight total sources (4 brain, 4 muscle). For this reason, we anticipated the possibility of over separating these sources during ICA. We therefore applied Principal Component Analysis data reduction during AMICA. To guide this decision, we performed AMICA on the cleanest condition (no motion, ± 0 μV muscle amplitude, 0.5 m/s brain signal input) without Principal Component Analysis reduction, and with Principal Component Analysis reduction set to 15, 30, 60, and the number of combined scalp EEG and EMG channels remaining after preprocessing. For each Principal Component Analysis reduction cutoff, we calculated the trial-averaged root mean square error to find the best-matched sources compared to the ground-truth. This testing identified that Principal Component Analysis reduction to 15 components returned the lowest average root mean square error values, therefore we applied this criterion to each subsequent analysis.

As a final step, we performed AMICA on the simulated EEG data after applying the best-practice artifact removal approaches from aims 1-4 during head motions at each walking speed. This was done separately for each muscle amplitude condition to assess the combined performance of motion and muscle artifact removal methods for isolating the ground-truth artificial electrocortical sources. In each case, Artifact Subspace Reconstruction preprocessing was applied to the scalp EEG channels, followed by Canonical Correlation Analysis.

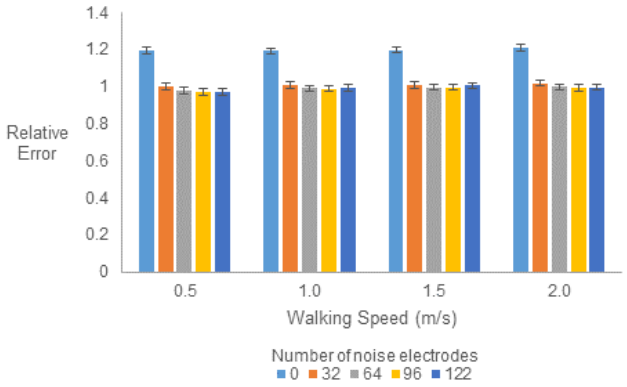

Fig. 2. Average relative error of the four best-fit components at each walking speed during motion, but without muscle activity. Relative error >1 indicates the error exceeds the ground-truth spectral power fluctuations, 1 indicates equivalent error and ground-truth signal spectral power fluctuations, <1 indicates the error is less than the ground-truth spectral power fluctuations, 0 indicates no error between component and ground-truth. ICA input included scalp EEG channel recordings and different subsets of isolated noise channel recordings (0, 32, 64, 96, and all 122 remaining) as separate rows of the data matrix. Including noise electrodes improved source separation but including a larger subset of electrodes did not further reduce relative error values. Error bars represent 99% confidence intervals.

The preprocessed EEG channels were used as the ICA input, with isolated noise and neck EMG channels stacked below as separate rows of the data matrix.

E. Statistical Analyses

We averaged the inter-trial variability from the relative error values in each gait cycle to define 99% confidence intervals surrounding the condition mean (adjusted to the number of possible comparisons in each sub-analysis). The confidence interval of the relative error averaged among the four best-fit components in each condition were therefore calculated using equation (1):

$$Confidence\ Interval = \frac{zscore * SD}{\sqrt{(n)}} \tag{1}$$

Here, z score was set to 2.576, SD represents the averaged standard deviation among gait cycles for the four best-fit components, and n is the number of gait cycles in the condition. Non-overlapping confidence intervals suggest statistically significant source signal recovery differences in contrasting hardware configurations and signal processing schemes.

III. Results

A. Aim 1: Dual Layer EEG Noise Sensor Recordings for Motion Artifact Removal

By including isolated noise sensor recordings in the ICA decomposition of high-density mobile EEG data during motion, we saw improved source separation based on comparisons to ground-truth artificial electrocortical spectral power fluctuations (Fig. 2). In each gait speed condition, including any subset of isolated noise channel recordings (32, 64, 96, or 122 channels) reduced the relative error values compared to not including noise channel data the ICA decomposition. Including a larger subset of the electrodes, however, did not further improve source signal recovery compared to using 32 noise channels during ICA. As few as 32 evenly distributed

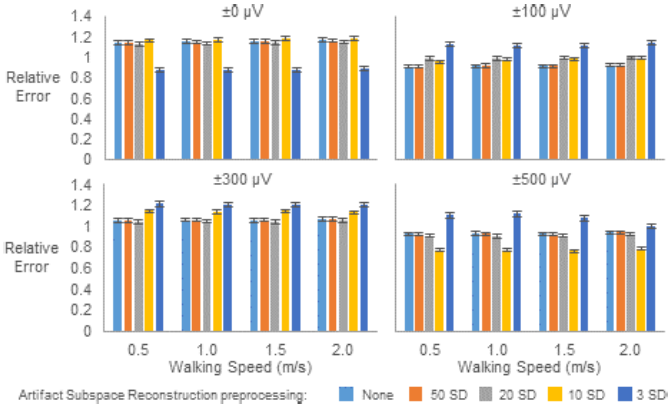

Fig. 3. Average relative error of the four best-fit components at each walking speed during head motion, and with muscle activity amplitudes set to ±0, 100, 300, and 500 μV. Relative error >1 indicates the error exceeds the ground-truth spectral power fluctuations, 1 indicates equivalent error and ground-truth signal spectral power fluctuations, <1 indicates the error is less than the ground-truth spectral power fluctuations, 0 indicates no error between component and ground-truth. ICA input only included EEG scalp channel recordings without or with Artifact Subspace Reconstruction preprocessing at thresholds of 50, 20, 10, or 3 standard deviations (SD) from baseline. Muscle activity amplitude affected the effectiveness of Artifact Subspace Reconstruction (ASR). Error bars represent 99% confidence intervals.

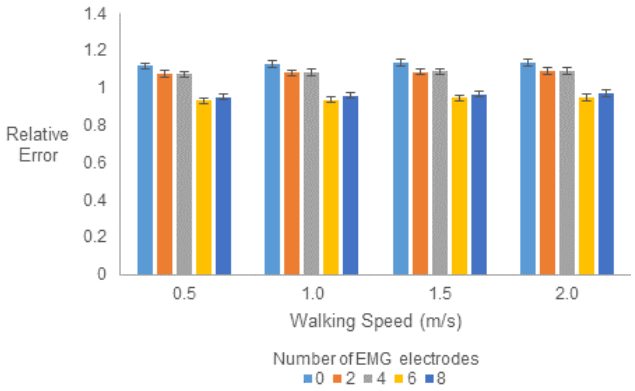

Fig. 4. Average relative error of the four best-fit components at each walking speed, without head motion, and with ±100 μV neck muscle activity amplitudes. Relative error >1 indicates the error exceeds the ground-truth spectral power fluctuations, 1 indicates equivalent error and ground-truth signal spectral power fluctuations, <1 indicates the error is less than the ground-truth spectral power fluctuations, 0 indicates no error between component and ground-truth. ICA input included scalp EEG channel recordings and different subsets of bilateral neck EMG recordings (0, 2, 4, 5, and 8 channels) as separate rows of the data matrix. Including 6 or 8 EMG electrodes provided the lowest relative error values. Error bars represent 99% confidence intervals.

isolated noise channels across the scalp were able to effectively capture and remove motion artifacts from high-density mobile EEG data during simulated human walking.

B. Aim 2: Artifact Subspace Reconstruction for Motion and Muscle Artifact Removal

In absence of muscle activity, Artifact Subspace Reconstruction applied with a 3 standard deviation threshold relative to baseline improved source signal recovery using ICA. This was evidenced by reduced relative error values compared to performing Artifact Subspace Reconstruction at higher standard deviation cutoffs, or without Artifact Subspace Reconstruction (Fig. 3, top left). When the EEG signals were contaminated by muscle activity, however, Artifact Subspace Reconstruction performance varied. In general, a strict Artifact Subspace Reconstruction threshold (3 standard deviations from baseline) led to increased relative error values compared to more lenient standard deviation thresholds, or to preprocessing without Artifact Subspace Reconstruction (Fig. 3). Artifact Subspace Reconstruction preprocessing therefore provided a possible advantage for motion artifact removal but showed inconsistencies during muscle artifact removal.

C. Aim 3: Neck EMG Sensor Recordings for Muscle Artifact Removal

By including neck EMG channel recordings in the high-density mobile EEG ICA decomposition, we saw improved source separation. This was indicated by reduced relative error values for the recovered sources compared to ground-truth artificial electrocortical spectral power fluctuations (Fig. 4). We detected progressive improvements in source signal recovery with additional neck EMG recordings included in ICA. Six or 8 neck EMG channels more effectively captured and removed muscle artifacts compared to reduced channel subsets, or to including no EMG recordings in ICA.

D. Aim 4: Canonical Correlation Analysis for Muscle Artifact Removal

Performing Canonical Correlation Analysis and removing artifact components from muscle-activity contaminated EEG data improved source signal recovery (Fig. 5). This was demonstrated by reduced relative error compared to ICA source separation without Canonical Correlation Analysis preprocessing in the condition without muscle artifact contamination. Artificial brain source recovery improved in ±100 and 500 μV muscle activity amplitude conditions compared to artifact free and ±300 μV conditions.

E. Combined Motion and Muscle Artifact Removal Methods

Based on the results from aims 1-4, we processed the high-density mobile EEG during head motions at each walking speed. This was done separately for each neck muscle activity amplitude condition (±100, 300, 500 μV). In the combined analyses, we included 32-isolated noise channel recordings (Aim 1) and 8-neck EMG channel recordings (Aim 3) in the ICA decomposition, along with the preprocessed scalp EEG channel data, as separate rows of the input matrix. Because we did not find a conclusive best Artifact Subspace Reconstruction threshold (Aim 2), we applied a 20 standard deviation cutoff from baseline because it has been used and recommended in previous studies [11], [16]. Following Artifact Subspace Reconstruction preprocessing, we performed Canonical Correlation Analysis (Aim 4) to remove residual muscle artifacts from the scalp EEG channels.

Table I shows the relative error values for the averaged electrocortical sources, at each muscle activity amplitude (±100, 300, and 500 μV) and walking speed condition (0.5, 1.0. 1.5, and 2.0 m/s). Relative error values were relatively consistent across walking speeds but increased in the ±300 and 500 μV muscle amplitude conditions relative to the

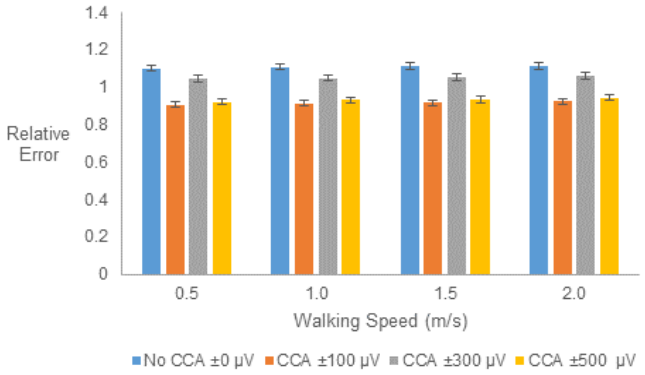

Fig. 5. Average relative error of the four best-fit components at each walking speed, without head motions. Relative error >1 indicates the error exceeds the ground-truth spectral power fluctuations, 1 indicates equivalent error and ground-truth signal spectral power fluctuations, <1 indicates the error is less than the ground-truth spectral power fluctuations, 0 indicates no error between component and ground-truth. The condition without neck muscle activity (0 μV) was not processed with Canonical Correlation Analysis (CCA), while ±100, 300, and 500 μV muscle amplitude conditions were processed with Canonical Correlation Analysis. Only EEG scalp channel recordings were included in the ICA decomposition with or without Canonical Correlation Analysis preprocessing. Canonical Correlation Analysis improved source separation in muscle-contaminated data compared to the ±0 μV condition processed without Canonical Correlation Analysis. It was less effective in the ±300 μV muscle amplitude condition compared to the ±100 and 500 μV conditions. Error bars represent 99% confidence intervals.

TABLE I
AVERAGE RELATIVE ERROR OF THE FOUR BEST-FIT COMPONENTS AFTER COMBINING BEST PRACTICE SIGNAL PROCESSING APPROACHES

	Relative error			
	0.5 m/s	1.0 m/s	1.5 m/s	2.0 m/s
±100 μV	0.76	0.76	0.77	0.78
±300 μV	0.91	0.91	0.91	0.92
±500 μV	0.91	0.92	0.92	0.93

Average relative error of the four best-fit components during head motions at each walking speed, and with ±100, 300, and 500 μV neck muscle activity amplitudes. Relative error >1 indicates the error exceeds the ground-truth spectral power fluctuations, 1 indicates equivalent error and ground-truth signal spectral power fluctuations, <1 indicates the error is less than the ground-truth spectral power fluctuations, 0 indicates no error between component and ground-truth. EEG-channel preprocessing included Artifact Subspace Reconstruction (20 standard deviation cutoff) and Canonical Correlation Analysis artifact component removal, with 32-isolated noise channels and 8-neck EMG channels stored as separate rows in the ICA input matrix. ICA source separation was similar across walking speeds but worsened at higher muscle activity amplitudes.

±100 μV condition, indicating worse artificial electrocortical source recovery. Fig. 6a shows separate event-related spectral perturbation plots from the four electrocortical sources during head motions walking at 1.5 m/s and with ±100 μV neck muscle activity amplitudes. From left to right, we show spectral power fluctuations from scalp EEG channel recordings in closest proximity to the source antennae (10-channel mean), ground-truth artificial electrocortical source activity, and best-fit components recovered by ICA. Fig. 6b shows exemplar noise channel recordings and Fig. 6c shows the ground-truth neck muscle activity.

IV. DISCUSSION

Using a conductive head phantom and robotic motion platform, we were able to evaluate the best practices for removing motion and muscle artifacts from human mobile dual layer EEG and neck EMG recordings. Broadcasting ground-truth artificial brain signals that were designed to simulate human electrocortical activity during walking, in conjunction with reproduced gait-related head motions and human neck muscle activity, allowed us to evaluate high-density 128-channel dual layer mobile EEG and 8-channel neck EMG recordings from the head phantom. This benchmark testing setup allowed us to determine: (1) the number of isolated noise sensor recordings needed to capture and remove motion artifacts, (2) the ability of Artifact Subspace Reconstruction to remove motion and muscle artifacts at contrasting artifact detection thresholds, (3) the number of neck EMG sensor recordings needed to capture and remove muscle artifacts, and (4) the ability of Canonical Correlation Analysis to remove muscle artifacts. As a result, we were then able to test the combined ability of these methods to recover ground-truth electrocortical spectral power fluctuations across the gait cycle.

In agreement with our hypotheses, (1) including isolated noise recordings from dual layer EEG sensors in the ICA decomposition with high-density scalp EEG data improved artificial electrocortical source signal recovery during motion (Fig. 2). As few as 32-isolated noise channels were able to capture and help remove the dominant motion-induced noise sources. Artifact Subspace Reconstruction preprocessing (2) improved source signal recovery during motion, when applied at a relatively strict standard deviation cutoff (3 standard deviations), but was less effective at removing muscle artifacts from scalp EEG data (Fig. 3). Muscle artifact removal, however, was improved by including up to 6- or 8-channel neck EMG recordings (3) in the ICA decomposition with scalp EEG data (Fig. 4). Canonical Correlation Analysis preprocessing for muscle artifact removal (4) showed improvements in artificial brain source separation from high-density mobile EEG-channel data (Fig. 5). Combining preprocessing methods from aims 2 and 4, and additional sensor data from aims 1 and 3, allowed us to isolate the artificial brain sources relatively cleanly, based on comparisons to the ground-truth electrocortical spectral power fluctuations across the gait cycle (Fig. 6). However, increased levels of neck muscle activity contamination compromised source signal recovery (Table I).

There was a clear benefit of using isolated noise channels to capture motion artifacts from high-density mobile EEG recordings. Simply by including these channels in the ICA decomposition, we were able to see improved source signal recovery compared to processing scalp EEG channels alone (Fig. 2). The benefits of the dual layer electrode array have been demonstrated both in benchmark head phantom experiments [17], [29] and human locomotion studies [12], [17]. Initial channel-based signal quality measures were quantified in Nordin *et al.* [29] using an 8-channel dual layer setup that showed limited motion artifact contamination compared to traditional single-layer scalp EEG recordings during vigorous

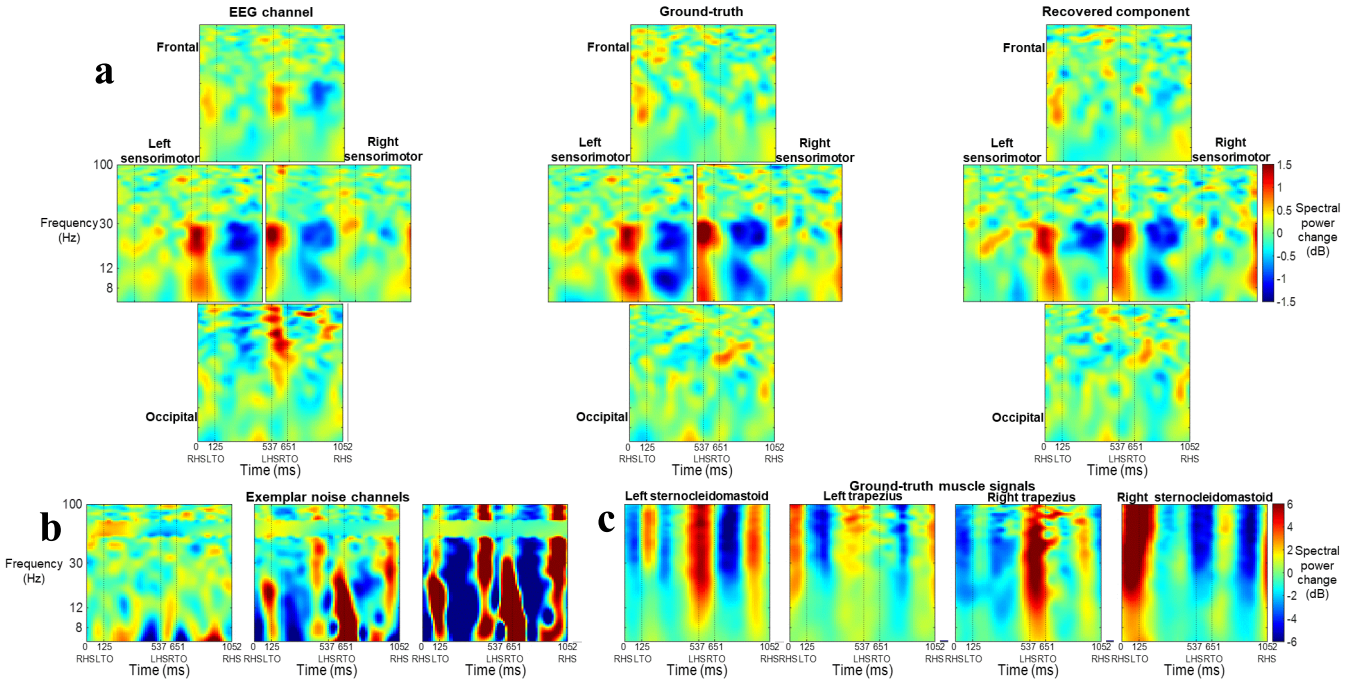

Fig. 6. a) Event-related spectral perturbation plots for the four brain sources during head motions walking at 1.5 m/s, with 100 μV neck muscle activity amplitude. (Left column) Average of the 10 EEG channels in closest proximity to each source, (Middle column) ground-truth electrocortical input signals, (Right column) best-fit recovered component from ICA. Combining best practice signal processing allowed ICA to recover components closely resembling the ground-truth. Sensorimotor gait-related activity was recovered both at the channel and component level. Best practice processing allowed for a better recovery of the frontal and occipital sources, which display artifact related spectral power fluctuations at the channel level that are absent from the ground-truth signals. b) Exemplar noise channel event-related spectral perturbation plots from the left, center, and right sides of the head. Spectral power fluctuation patterns were similar across the scalp but amplitudes differed among channels. Line noise is visible at 60 Hz in all noise channel recordings. c) Ground-truth muscle activity input signals that show lateralized activity tied to the gait events. R: right, L: left, HS: heel strike, TO: toe off.

head movements. The benefits of including isolated noise recordings from dual layer EEG hardware in the ICA decomposition along with scalp EEG recordings were subsequently demonstrated in Nordin *et al*. [17] using a 40-channel dual layer EEG setup. This hardware configuration allowed six temporally randomized and overlapping sinusoidal bursts to be cleanly recovered from an electrical head phantom during simulated human walking, only after including both the scalp EEG and isolated noise recordings in the ICA decomposition. Human locomotion experiments have since used dual layer EEG configurations that included 128 scalp EEG and 40 isolated noise electrodes. This setup expanded possibilities for signal processing schemes and led to the recovery of human electrocortical activity during obstacle navigation and the effects of gait speed on human brain dynamics [17]. Here, we assembled a complete 128-channel dual layer array to determine the number of isolated noise sensor recordings needed to capture and remove motion artifacts. Our results indicate that source recovery capabilities did not improve beyond 32 isolated noise channels (Fig. 2). It is, however, important to acknowledge that our head phantom contained only four artificial brain sources and an additional four neck muscle sources. The number of recording channels in relation to the number of neural sources could therefore have led to over separation of our neural signals. To compensate for this, we implemented Principal Component Analysis reduction to 15 components prior to ICA, but acknowledge the possibility that the limited number of neural sources in our head phantom may have favored the use of fewer sensors. Future experiments should examine a more complex dataset including more neural sources and contrasting levels of motion artifact, while also using smaller subsets of noise channels. Nevertheless, our results corroborate the use of limited isolated noise sensor subsets compared to the number of scalp EEG sensors for improving electrocortical source recovery during dynamic mobile EEG recordings [12], [17].

Artifact Subspace Reconstruction is commonly used to clean motion artifact-contaminated mobile EEG data [11], [12], [16], [20], [22], [23]. Because contrasting artifact detection thresholds have been used in human experiments, there is some uncertainty regarding the appropriate cutoff to use during artifact removal. An aggressive 3 standard deviation cutoff has been used in recent investigations [10], [22], [23], which has the potential to remove electrocortical activity along with artifacts [11]. For this reason, other researchers have chosen a more lenient 20 standard deviation threshold [11], [16], arguing that movement-related brain activity should not exceed 20 standard deviations from resting brain activity [11]. Chang *et al*. [21] recently evaluated the performance of Artifact Subspace Reconstruction for EEG artifact removal at contrasting standard deviation thresholds. The authors suggest that a 5-7 standard deviation cutoff could be overly aggressive, while a broad range from 10-100 standard deviations from baseline

limits the likelihood of removing electrocortical source activity along with transient, high amplitude artifacts [21]. Here, our use of an electrical head phantom for benchmark testing allowed us to carefully evaluate different Artifact Subspace Reconstruction thresholds with knowledge of the ground-truth neural activity. By applying Artifact Subspace Reconstruction at contrasting thresholds we found that source signal recovery was highly dependent on muscle artifact contamination amplitude. Without muscle activity contamination, a 3 standard deviation threshold returned the best matched electrocortical source activity relative to the ground-truth signal. When neck muscle contamination was present, however, aggressive cutoffs appeared to be detrimental to source recovery from ICA (Fig. 3). Because muscle activity is largely unavoidable during human mobile EEG collections, our results suggest an Artifact Subspace Reconstruction cutoff of 3 or even 10 standard deviations may be overly aggressive, in agreement with Chang and colleagues [21]. We must acknowledge, however, that our head phantom lacks a skull, skin, and hair layers that can allow neck muscle activity to be more broadly propagated throughout the homogenous head, but may limit artifacts induced by independent electrode motions on the scalp and hair. Additional motion artifact suppression due to dual layer EEG cable bundling and an overlaid secondary cap [12], [17], [29], along with filtered and robotically reproduced head trajectories could therefore have limited the potential benefits of Artifact Subspace Reconstruction preprocessing. This could explain the apparent advantage of a low standard deviation cutoff in EEG recordings without muscle artifacts, but the apparent disadvantage in conditions with muscle artifacts. Compared to human mobile EEG recordings, the limited number of neural sources contributing to the recorded scalp potentials could also limit the efficacy of this PCA-based artifact removal approach, because a large proportion of the signal is captured in a small number of components.

Muscle artifact removal benefitted from the inclusion of neck EMG recordings capturing sources of muscle contamination in the scalp EEG sensors. Similar to our use of isolated noise recordings for extracting motion artifacts from EEG channel data, direct muscle activity measures assisted in the separation of ground-truth electrocortical source activity during ICA. This approach has previously been used in human data collections [12], [17], [31] and our results confirm its usefulness. Further, applying Canonical Correlation Analysis to scalp EEG recordings helped remove muscle artifacts by separating high and low frequency components of the EEG signals based on autocorrelation (Fig. 5). Multiple researchers have now demonstrated the ability of Canonical Correlation Analysis to isolate high-frequency muscle contamination [12], [16], [27], [32], [33]. Safieddine *et al*. [32] compared muscle artifact removal methods in computer simulations and found that Canonical Correlation Analysis performed better when muscle artifact contamination was less severe. Our results partially align with these findings, because the advantage of Canonical Correlation Analysis was greater in the $\pm$100-μV-muscle amplitude condition compared to the $\pm$300-μV-muscle amplitude condition, however performance was similar between $\pm$100 and 500-μV-muscle amplitude conditions (Fig. 5). Encouragingly, we observe clear improvements in the $\pm$100-μV-muscle amplitude condition, which reflects muscle activity amplitudes measured during human walking [12]. As a result, Canonical Correlation Analysis provides a valuable tool for muscle artifact removal in human mobile EEG studies.

Combining best practice signal processing approaches from aims 1-4, we were able to recover ground-truth artificial electrocortical signals during head motions at a range of walking speeds, and with contrasting levels of muscle activity contamination. High density mobile EEG preprocessed with Artifact Subspace Reconstruction and Canonical Correlation Analysis, in addition to the inclusion of 32 isolated noise and 8 neck EMG channels in the ICA decomposition, recovered source components that closely resembled ground-truth input signals (Fig. 6a). ICA recovery of the right sensorimotor electrocortical source was nearly identical to the ground-truth spectral power fluctuations. Left sensorimotor spectral power fluctuations also showed close similarity to the ground-truth signal in beta band (12-30 Hz). Some signal loss, however, was evident in the left sensorimotor source within delta, theta, and alpha bands ($<$12 Hz, Fig. 6a). Frontal and occipital best-fit components closely resemble their ground-truth source activity, which did not contain gait-related activity. At the EEG channel level, however, we observed artifact contamination in the frontal and occipital areas. Across gait speeds, ICA source separation showed consistent motion and muscle artifact removal performance that worsened at muscle amplitudes exceeding those typically measured in human walking ($\pm$300 and 500 μV, Table I). Although electrocortical source recovery suffered at increased levels of muscle activity contamination, the combined artifact removal methods revealed the lowest relative error value in the $\pm$100-μV-muscle activity amplitude condition, compared to any of the individual analyses in aims 1-4. This suggests that our combined artifact removal methods can outperform the individual methods in isolation, which is informative for human mobile EEG processing pipelines [12]. Nevertheless, there are limitations in our ability to directly transfer these findings to human EEG analyses. Our use of Principal Component Analysis reduction to 15 components is well below that of typical human EEG processing and could compromise the subsequent ICA decomposition [43]. We applied these criteria due to the limited number of sources in our head phantom and our need to compare each component to the ground-truth signal after time-frequency analysis. Further, despite adding neck muscle activity and more realistic artificial brain signals to our head phantom, along with spectral power fluctuations that matched gait events, our setup still lacks the complexity of the human brain and additional sources of physiological contamination. We need to continue to develop increasingly complex head phantom devices with physiologically realistic input signals including facial muscles, eyes movements, and heartbeat to improve mobile brain imaging validation methods. Future work should also increase the number of cortical sources to find an optimal configuration for a more realistic phantom.

V. Conclusion

Our approach of broadcasting ground-truth artificial brain signals through an electrical head phantom that reproduced head trajectories from human walking helped validate mobile EEG motion and muscle artifact removal methods. Dual layer EEG allowed us to confirm that source signal recovery can be improved by including as few as 32-isolated noise channel recordings in the ICA decomposition with high-density EEG. Additionally, Artifact Subspace Reconstruction was useful for cleaning motion artifact contaminated EEG. Muscle artifacts, however, were more effectively removed by including EMG sensor recordings in the ICA decomposition and through Canonical Correlation Analysis preprocessing of EEG channel data. In combination, Artifact Subspace Reconstruction preprocessing, Canonical Correlation Analysis preprocessing, and the inclusion of isolated noise and EMG recordings in ICA are effective tools for cleaning motion and muscle artifacts from high-density mobile EEG data. These findings contribute to our understanding of best practices for mobile EEG hardware configurations and signal processing.

References

[1] P. M. R. Reis, F. Hebenstreit, F. Gabsteiger, V. von Tscharner, and M. Lochmann, "Methodological aspects of EEG and body dynamics measurements during motion," *Frontiers Hum. Neurosci.*, vol. 8, p. 156, Mar. 2014.

[2] J. E. Kline, H. J. Huang, K. L. Snyder, and D. P. Ferris, "Isolating gait-related movement artifacts in electroencephalography during human walking," *J. Neural Eng.*, vol. 12, no. 4, Aug. 2015, Art. no. 046022.

[3] K. L. Snyder, J. E. Kline, H. J. Huang, and D. P. Ferris, "Independent component analysis of gait-related movement artifact recorded using EEG electrodes during treadmill walking," *Frontiers Hum. Neurosci.*, vol. 9, p. 639, Dec. 2015.

[4] J. T. Gwin, K. Gramann, S. Makeig, and D. P. Ferris, "Electrocortical activity is coupled to gait cycle phase during treadmill walking," *NeuroImage*, vol. 54, no. 2, pp. 1289–1296, Jan. 2011.

[5] J. Wagner, T. Solis-Escalante, P. Grieshofer, C. Neuper, G. Müller-Putz, and R. Scherer, "Level of participation in robotic-assisted treadmill walking modulates midline sensorimotor EEG rhythms in able-bodied subjects," *NeuroImage*, vol. 63, no. 3, pp. 1203–1211, Nov. 2012.

[6] M. Seeber, R. Scherer, J. Wagner, T. Solis-Escalante, and G. R. Müller-Putz, "EEG beta suppression and low gamma modulation are different elements of human upright walking," *Frontiers Hum. Neurosci.*, vol. 8, pp. 1–9, Jul. 2014.

[7] M. Seeber, R. Scherer, J. Wagner, T. Solis-Escalante, and G. R. Müller-Putz, "High and low gamma EEG oscillations in central sensorimotor areas are conversely modulated during the human gait cycle," *NeuroImage*, vol. 112, pp. 318–326, May 2015.

[8] J. C. Bradford, J. R. Lukos, and D. P. Ferris, "Electrocortical activity distinguishes between uphill and level walking in humans," *J. Neurophysiol.*, vol. 115, no. 2, pp. 958–966, Feb. 2016.

[9] A. S. Oliveira, B. R. Schlink, W. D. Hairston, P. König, and D. P. Ferris, "Restricted vision increases sensorimotor cortex involvement in human walking," *J. Neurophysiol.*, vol. 118, no. 4, pp. 1943–1951, Oct. 2017.

[10] T. C. Bulea, J. Kim, D. L. Damiano, C. J. Stanley, and H.-S. Park, "Prefrontal, posterior parietal and sensorimotor network activity underlying speed control during walking," *Frontiers Hum. Neurosci.*, vol. 9, p. 247, May 2015.

[11] F. Artoni, C. Fanciullacci, F. Bertolucci, A. Panarese, S. Makeig, S. Micera, and C. Chisari, "Unidirectional brain to muscle connectivity reveals motor cortex control of leg muscles during stereotyped walking," *NeuroImage*, vol. 159, pp. 403–416, Oct. 2017.

[12] A. D. Nordin, W. D. Hairston, and D. P. Ferris, "Faster gait speeds reduce alpha and beta EEG spectral power from human sensorimotor cortex," *IEEE Trans. Biomed. Eng.*, vol. 67, no. 3, pp. 842–853, Mar. 2020.

[13] J. A. Urigüen and B. Garcia-Zapirain, "EEG artifact removal—State-of-the-art and guidelines," *J. Neural Eng.*, vol. 12, no. 3, Jun. 2015, Art. no. 031001.

[14] J. T. Gwin, K. Gramann, S. Makeig, and D. P. Ferris, "Removal of movement artifact from high-density EEG recorded during walking and running," *J. Neurophysiol.*, vol. 103, no. 6, pp. 3526–3534, Jun. 2010.

[15] S. M. Peterson and D. P. Ferris, "Combined head phantom and neural mass model validation of effective connectivity measures," *J. Neural Eng.*, vol. 16, no. 2, Apr. 2019, Art. no. 026010.

[16] S. M. Peterson and D. P. Ferris, "Differentiation in theta and beta electrocortical activity between visual and physical perturbations to walking and standing balance," *Eneuro*, vol. 5, no. 4, 2018.

[17] A. D. Nordin, W. D. Hairston, and D. P. Ferris, "Human electrocortical dynamics while stepping over obstacles," *Sci. Rep.*, vol. 9, no. 1, p. 4693, Dec. 2019.

[18] B. W. McMenamin, A. J. Shackman, L. L. Greischar, and R. J. Davidson, "Electromyogenic artifacts and electroencephalographic inferences revisited," *NeuroImage*, vol. 54, no. 1, pp. 4–9, Jan. 2011.

[19] A. S. Oliveira, B. R. Schlink, W. D. Hairston, P. König, and D. P. Ferris, "Induction and separation of motion artifacts in EEG data using a mobile phantom head device," *J. Neural Eng.*, vol. 13, no. 3, Jun. 2016, Art. no. 036014.

[20] T. Mullen, C. Kothe, Y. M. Chi, A. Ojeda, T. Kerth, S. Makeig, G. Cauwenberghs, and T.-P. Jung, "Real-time modeling and 3D visualization of source dynamics and connectivity using wearable EEG," in *Proc. 35th Annu. Int. Conf. IEEE Eng. Med. Biol. Soc. (EMBC)*, Jul. 2013, pp. 2184–2187.

[21] C.-Y. Chang, S.-H. Hsu, L. Pion-Tonachini, and T.-P. Jung, "Evaluation of artifact subspace reconstruction for automatic EEG artifact removal mental health monitoring with EEG view project evaluation of artifact subspace reconstruction for automatic EEG artifact removal," in *Proc. 40th Annu. Int. Conf. IEEE Eng. Med. Biol. Soc. (EMBC)*, Jul. 2018, pp. 1242–1245.

[22] T. P. Luu, J. A. Brantley, S. Nakagome, F. Zhu, and J. L. Contreras-Vidal, "Electrocortical correlates of human level-ground, slope, and stair walking," *PLoS ONE*, vol. 12, no. 11, pp. 1–15, 2017.

[23] T. P. Luu, S. Nakagome, Y. He, and J. L. Contreras-Vidal, "Real-time EEG-based brain-computer interface to a virtual avatar enhances cortical involvement in human treadmill walking," *Sci. Rep.*, vol. 7, no. 1, pp. 1–12, Dec. 2017.

[24] K. Al-Subari, S. Al-Baddai, A. M. Tomé, M. Goldhacker, R. Faltermeier, and E. W. Lang, "EMDLAB: A toolbox for analysis of single-trial EEG dynamics using empirical mode decomposition," *J. Neurosci. Methods*, vol. 253, pp. 193–205, Sep. 2015.

[25] Z. Wu and N. E. Huang, "Ensemble empirical mode decomposition: A noise-assisted data analysis method," *Adv. Adapt. Data Anal.*, vol. 1, no. 1, pp. 1–41, Jan. 2009.

[26] H. Hotelling, "Relations between two sets of variates," *Biometrika*, vol. 28, nos. 3–4, pp. 321–377, Dec. 1936.

[27] V. Roy, S. Shukla, P. K. Shukla, and P. Rawat, "Gaussian elimination-based novel canonical correlation analysis method for EEG motion artifact removal," *J. Healthcare Eng.*, vol. 2017, Oct. 2017, Art. no. 9674712.

[28] E.-R. Symeonidou, A. Nordin, W. Hairston, and D. Ferris, "Effects of cable sway, electrode surface area, and electrode mass on electroencephalography signal quality during motion," *Sensors*, vol. 18, no. 4, p. 1073, Apr. 2018.

[29] A. D. Nordin, W. D. Hairston, and D. P. Ferris, "Dual-electrode motion artifact cancellation for mobile electroencephalography," *J. Neural Eng.*, vol. 15, no. 5, Oct. 2018, Art. no. 056024.

[30] R. L. Cromwell, T. K. Aadland-Monahan, A. T. Nelson, S. M. Stern-Sylvestre, and B. Seder, "Sagittal plane analysis of head, neck, and trunk kinematics and electromyographic activity during locomotion," *J. Orthopaedic Sports Phys. Therapy*, vol. 31, no. 5, pp. 255–262, May 2001.

[31] N. Richer, R. J. Downey, A. D. Nordin, W. D. Hairston, and D. P. Ferris, "Adding neck muscle activity to a head phantom device to validate mobile EEG muscle and motion artifact removal," in *Proc. 9th Int. IEEE/EMBS Conf. Neural Eng. (NER)*, Mar. 2019, pp. 275–278.

[32] D. Safieddine *et al.*, "Removal of muscle artifact from EEG data: Comparison between stochastic (ICA and CCA) and deterministic (EMD and wavelet-based) approaches," *EURASIP J. Adv. Signal Process.*, vol. 2012, no. 1, p. 127, Dec. 2012.

[33] A. S. Janani, T. S. Grummett, T. W. Lewis, S. P. Fitzgibbon, E. M. Whitham, D. DelosAngeles, H. Bakhshayesh, J. O. Willoughby, and K. J. Pope, "Improved artefact removal from EEG using canonical correlation analysis and spectral slope," *J. Neurosci. Methods*, vol. 298, pp. 1–15, Mar. 2018.

[34] A. Yu and W. D. Hairston. (2019). *Open EEG Phantom*. [Online]. Available: https://osf.io/qrka2/

[35] A. B. Yu, C. G. Sinks, and W. D. Hairston, "Easily fabricated phantom heads for EEG signal and hardware validation," in *Proc. Int. IEEE EMBS Conf. Neural Eng. (EMBS NER)*, San Francisco, CA, USA, 2019.

[36] W. David Hairston, G. A. Slipher, and A. B. Yu, "Ballistic gelatin as a putative substrate for EEG phantom devices," 2016, *arXiv:1609.07691*. [Online]. Available: http://arxiv.org/abs/1609.07691

[37] A. I. Farrer, H. Odéen, J. de Bever, B. Coats, D. L. Parker, A. Payne, and D. A. Christensen, "Characterization and evaluation of tissue-mimicking gelatin phantoms for use with MRgFUS," *J. Therapeutic Ultrasound*, vol. 3, no. 1, p. 9, Dec. 2015.

[38] D. Richler and D. Rittel, "On the testing of the dynamic mechanical properties of soft gelatins," *Exp. Mech.*, vol. 54, no. 5, pp. 805–815, Jun. 2014.

[39] O. David and K. J. Friston, "A neural mass model for MEG/EEG: Coupling and neuronal dynamics," *NeuroImage*, vol. 20, no. 3, pp. 1743–1755, Nov. 2003.

[40] M. M. Vindiola, J. M. Vettel, S. M. Gordon, P. J. Franaszczuk, and K. McDowell, "Applying EEG phase synchronization measures to non-linearly coupled neural mass models," *J. Neurosci. Methods*, vol. 226, pp. 1–14, Apr. 2014.

[41] A. Delorme and S. Makeig, "EEGLAB: An open source toolbox for analysis of single-trial EEG dynamics including independent component analysis," *J. Neurosci. Methods*, vol. 134, no. 1, pp. 9–21, Mar. 2004.

[42] J. Palmer, K. Kreutz-Delgado, and S. Makeig, "AMICA: An adaptive mixture of independent component analyzers with shared components," Swartz Center Comput. Neursosci., San Diego, CA, USA, Tech. Rep., 2012, pp. 1–15. [Online]. Available: https://api.semanticscholar.org/CorpusID:11240515

[43] F. Artoni, A. Delorme, and S. Makeig, "Applying dimension reduction to EEG data by principal component analysis reduces the quality of its subsequent independent component decomposition," *NeuroImage*, vol. 175, pp. 176–187, Jul. 2018.